Cavitation transition in the energy landscape: Distinct tensile yielding behavior in strongly and weakly attractive systems

Y. Elia Altabet, Andreia L. Fenley, Frank H. Stillinger, and Pablo G. Debenedetti

---

Articles you may be interested in

Comprehensive representation of the Lennard-Jones equation of state based on molecular dynamics simulation data
The Journal of Chemical Physics 148, 114505 (2018); 10.1063/1.5021560

Perspective: Outstanding theoretical questions in polymer-nanoparticle hybrids
The Journal of Chemical Physics 147, 020901 (2017); 10.1063/1.4990501

Perspective: Surface freezing in water: A nexus of experiments and simulations
The Journal of Chemical Physics 147, 060901 (2017); 10.1063/1.4985879

Vitrification and gelation in sticky spheres
The Journal of Chemical Physics 148, 044501 (2018); 10.1063/1.5000263

Communication: Simple liquids' high-density viscosity
The Journal of Chemical Physics 148, 081101 (2018); 10.1063/1.5022058

Another resolution of the configurational entropy paradox as applied to hard spheres
The Journal of Chemical Physics 147, 224503 (2017); 10.1063/1.4999483
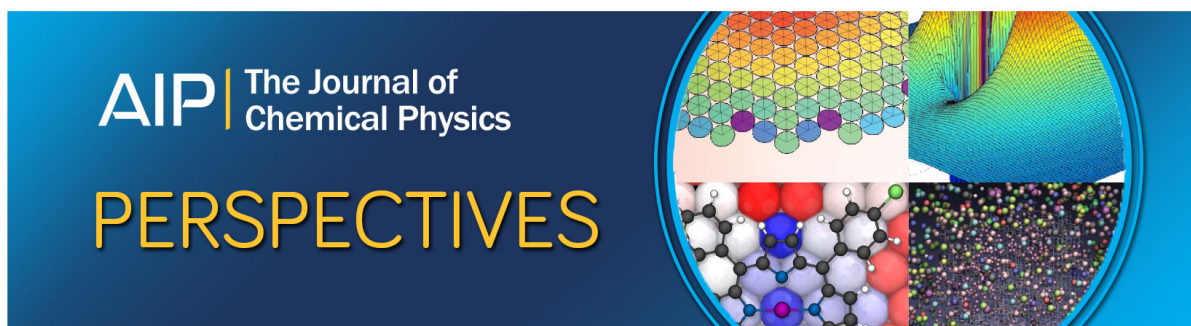
Cavitation transition in the energy landscape: Distinct tensile yielding behavior in strongly and weakly attractive systems

Y. Elia Altabet,[1] Andreia L. Fenley,[1] Frank H. Stillinger,[2] and Pablo G. Debenedetti[1,a)]

[1]*Department of Chemical and Biological Engineering, Princeton University, Princeton, New Jersey 08544, USA*
[2]*Department of Chemistry, Princeton University, Princeton, New Jersey 08544, USA*

Particles with cohesive interactions display a tensile instability in the energy landscape at the Sastry density ρ_S. The signature of this tensile limit is a minimum in the landscape equation of state, the pressure–density relationship of inherent structures sampled along a liquid isotherm. Our previous work [Y. E. Altabet, F. H. Stillinger, and P. G. Debenedetti, J. Chem. Phys. **145**, 211905 (2016)] revisited the phenomenology of Sastry behavior and found that the evolution of the landscape equation of state with system size for particles with interactions typical of molecular liquids indicates the presence of an athermal first-order phase transition between homogeneous and fractured inherent structures, the latter containing several large voids. Here, we study how this tensile limit manifests itself for different interparticle cohesive strengths and identify two distinct regimes. Particles with sufficiently strong cohesion display an athermal first-order phase transition, consistent with our prior characterization. Weak cohesion also displays a tensile instability. However, the landscape equation of state for this regime is independent of system size, suggesting the absence of a first-order phase transition. An analysis of the voids suggests that yielding in the energy landscape of weakly cohesive systems is associated with the emergence of a highly interconnected network of small voids. While strongly cohesive systems transition from exclusively homogeneous to exclusively fractured configurations at ρ_S in the thermodynamic limit, this interconnected network develops gradually, starting at ρ_S, even at infinite system size. *Published by AIP Publishing.* https://doi.org/10.1063/1.5019274

I. INTRODUCTION

While a substantial portion of the physics of dense simple liquids is well described by a system of particles with exclusively repulsive interactions,[1,2] such systems do not have distinct liquid and vapor phases. Rather, they exhibit a single fluid phase that can undergo isothermal decompression without the occurrence of a phase transition. Systems composed of particles with attractive interactions, when decompressed along a subcritical isotherm, will cavitate at sufficiently low densities, and the pressure will abruptly jump to the coexistence pressure. Such differences also appear to translate to a particle systems' athermal phase behavior. Two means of considering such behavior are sampling through athermal expansion or by producing an ensemble of energy-minimized configurations, often called inherent structures,[3–5] from a liquid sampled along an isotherm. Specifically, particles with and without cohesive interactions exhibit rather distinct landscape equations of state, defined as the pressure–density (P–ρ) relationship of the inherent structures.

Particles with exclusively repulsive interactions have a landscape equation of state which decreases monotonically upon decompression. Sufficient decompression results in energy-minimized structures where all the particles can distance themselves beyond the assigned range of mutual interaction. At this density and below, the pressure and potential energy are zero. The density where the pressure becomes zero is often called the jamming threshold and serves as the focal point of the jamming scenario for granular materials.[6–10]

Particles with attractive interactions will exhibit what has been called Sastry behavior.[11] Upon decompression, the inherent structures of attractive particle systems will begin to exhibit isotropic tension (i.e., negative pressure) yet still maintain spatial homogeneity. Further decompression will produce greater tensions until reaching a mechanical instability at the Sastry point, which is defined by the corresponding limiting negative pressure P_S and density ρ_S. Below ρ_S, the inherent structures relieve tension upon decompression. The tensile instability at ρ_S is due to cavitation in the inherent structures. We note that when sampling along a liquid isotherm, cavitation in the liquid can be well separated from cavitation in the energy landscape. In other words, a liquid configuration that appears homogeneous can have an inherent structure that is inhomogeneous due to cavitation. For finite systems, the landscape equation of state is akin to a mean-field liquid isotherm passing through a spinodal, a feature that has been observed for a variety of attractive particle systems.[12–21] The Sastry point was therefore interpreted as a spinodal-like point that separates homogeneous and cavitated inherent structures.[11,22]

We recently revisited the phenomenology of Sastry behavior for a binary Lennard-Jones mixture and found that it was subject to considerable finite-size effects.[23] While the

a)Author to whom correspondence should be addressed: pdebene@princeton.edu

landscape equation of state appears to contain a spinodal-like point at small system sizes, it becomes a discontinuous point in the thermodynamic limit. This discontinuity at ρ_S is the result of an abrupt transition in the liquid. Just above ρ_S, the liquid samples basins of attraction with minima that are homogeneous and under significant tension. Just below, the liquid exclusively samples basins with fractured inherent structures at much reduced tension. This dependence of the landscape equation of state upon system size is analogous to finite-size rounding of the thermal liquid/bubble transition.[24–27] We performed a finite-size scaling analysis that suggests that the finite-system size deviation of the characteristic density for this athermal transition scales with $1/N^{1/3}$, where N is the number of particles. Rather than a spinodal-like point, Sastry behavior for molecular liquids is more akin to an athermal first-order phase transition.

There appear to be two types of limiting mechanical behavior in the energy landscape, depending on the presence of attractive interactions. Particles with exclusively repulsive interactions, typical of granular systems, have a jamming threshold, above which the mechanically stable packings develop a yield stress.[9] Particles with strong attractive interactions, typical of molecular liquids, have a Sastry density, above which the inherent structures are homogeneous and below which they are fractured. The present work addresses the limiting mechanical behavior of amorphous materials for intermediate strengths of cohesion, between the two limits delineated above. Particles with such intermediate interactions include colloids, proteins, and buckyballs,[28,29] which can exhibit vapor/liquid phase behavior that is metastable with respect to fluid/crystal coexistence, a result of their short-ranged attractive interactions. A corollary to this work is that it also addresses whether jamming is unique to repulsive particles or instead more general to some classes of cohesive particles.

In this paper, we study the mechanical limits of inherent structures produced along liquid isotherms as a function of cohesive strength among the particles. Specifically, we study a binary mixture interacting via a (7, 6) Lennard-Jones potential (described in Sec. II) and vary the cutoff as a means of adjusting cohesive strength. In Sec. III, we show that for cohesive strengths above certain threshold, the landscape equation of state exhibits a response to system size that is consistent with the athermal cavitation transition we previously presented.[23] Section IV shows that particles with sufficiently weak cohesion still have a tensile instability in their landscape equation of state. However, their response to system size is weak or entirely absent, suggesting the absence of a first-order phase transition. The evolution of the pressure distribution upon crossing ρ_S suggests that for strong cohesion failure in the energy landscape is sudden, while systems composed of sufficiently weak particles fail gradually. Section V analyzes the size and connectivity of voids formed in the two distinct cohesive regimes. Strong cohesion results in the formation of several large voids. Yielding for weak cohesion is associated with the emergence of a small number of small voids that grow in number and become highly interconnected upon further decompression. Section VI contains concluding remarks as well as suggestions for further study.

II. METHODS

A. Interaction potential

We employ a recently introduced[30] generalized (n, 6) Lennard-Jones pair potential

$$\phi(r) = 4\epsilon \left[\lambda \left(\frac{\sigma}{r} \right)^n - \alpha \left(\frac{\sigma}{r} \right)^6 \right]. \quad (1)$$

The coefficients λ and α are defined as

$$\lambda = \frac{3}{2} \left(\frac{2^{n/6}}{n-6} \right), \quad \alpha = \frac{n}{2(n-6)} \quad (2)$$

and are designed such that, upon varying n, the location of the minimum and depth of the well are unchanged with respect to the values for the standard (12, 6) Lennard-Jones potential without a cutoff. Our previous work on the Sastry phenomenology[23] found that the softer (7, 6) variant exhibited clear features of a first-order phase transition in the energy landscape (e.g., a bimodal pressure distribution) at smaller system sizes than the traditional (12, 6) variant. Thus, we have limited the scope of this work to focus on the (7, 6) variant.

Here, we employ a cutoff r_c with force shifting of the potential to ensure that both the potential and the force between two particles is zero at the cutoff and beyond. The force shifted potential is given by

$$\phi^{fs}(r) = \begin{cases} \phi(r) - \phi(r_c) - (r - r_c)\phi'(r_c) & r \le r_c \\ 0 & r > r_c \end{cases}. \quad (3)$$

Reducing r_c has the effect of weakening the strength of the attractive interactions, as it reduces the well-depth. Below a certain r_c, 1.2828 for the (7, 6) variant, $\phi^{fs}(r)$ will be exclusively repulsive. To examine how the strength of intermolecular attractions affects yielding in the energy landscape, we have varied r_c between 1.4 and 3.5, specifically considering $r_c = 1.4, 1.5, 1.6, 1.7, 1.8, 1.9, 2.0, 2.5,$ and 3.5. Figure 1 plots $\phi^{fs}(r)$ for these values of r_c.

B. Simulation details

In this work, we study a glass forming system, a binary 50:50 mixture with the Wahnström[31] parameters: $\epsilon_{AA} = 1.0$,
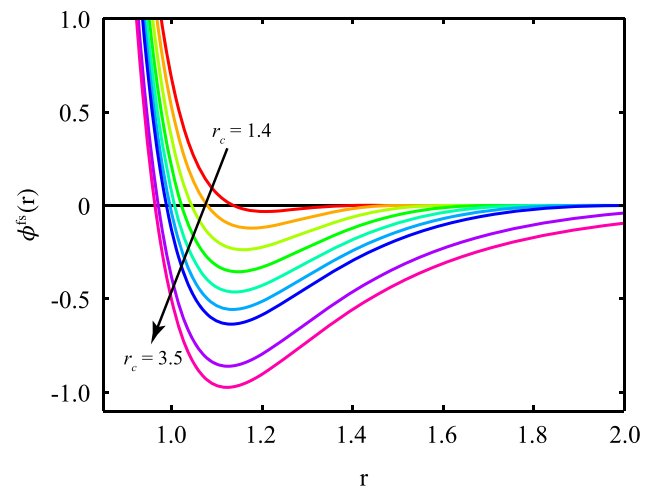
FIG. 1. Pair potential for each cutoff r_c considered in this work. Changing r_c changes the well depth and the extent of the attractive tail, allowing one to use r_c to tune the strength of particle cohesion.

$\sigma_{AA} = 1.0$; $\epsilon_{AB} = 1.0$, $\sigma_{AB} = 1.1$; $\epsilon_{BB} = 1.0$, $\sigma_{BB} = 1.2$. We report results in the traditional reduced units in terms of the *AA* interaction parameters.

Molecular dynamics is performed in a cubic simulation box with periodic boundary conditions in the canonical (NVT) ensemble at temperature $T = 1.0$. Time integration is performed via the velocity Verlet algorithm with molecular dynamics time step of 0.002 with the LAMMPS[32] software package. Simulations performed at fixed temperature employ a Nosé-Hoover thermostat.[33,34] Inherent structures are generated through energy minimization at fixed density using the Polak and Ribiere[35] method of conjugate gradients. Minimization was considered complete if the relative change in energy per iteration was less than 10^{-8}. All images of simulation configurations are rendered in Visual Molecular Dynamics (VMD).[36]

C. Generating inherent structures in systems with finite-ranged interactions

The conventional representation of particle systems in terms of the topography of their potential energy landscapes identifies inherent structures and their surrounding basins in a way that leads to an enumeration of those configurational features rising exponentially with system size.[37] However, introduction of a numerically simplifying assumption that potential energy contributions vanish identically beyond a finite cutoff distance r_c creates a conceptual ambiguity for inherent structures. Fortunately, this ambiguity has negligible effect for the densities used in the calculations reported in this paper. Nevertheless, at a very low density, the conjugate-gradient process applied to the potential energy landscape with a cutoff r_c would typically terminate at a configuration containing isolated single particles and/or isolated small clusters that are beyond the range of attractions to the remaining set of particles. In terms of the potential energy landscape itself, this involves continuous configurational subsets along which the system's potential energy is precisely constant. Any point within such regions of the landscape can serve as a termination of the conjugate gradient minimization process. If such termination configurations were to be defined as "inherent structures," they would be infinite in number for finite N and would "reside" in vanishingly small basins.

However, it should be noted that a definition of proper inherent structures as true local minima even in such low-density, cutoff-interaction situations can be implemented. In particular, this involves defining all points along an r_c-generated constant-potential configuration subset as being part of the basin belonging to the nearest mechanically stable potential energy minimum (i.e., the nearest conventional inherent structure). Thus, the respective portions of the constant-potential configuration subsets contribute to the anharmonic vibrational properties of their containing basins.

D. Void properties calculation

To study the void space in the inherent structures, we employ an algorithm based on Dong and Blunt's[38] modified maximal ball algorithm.[39] In this method, voids are identified by finding a set of the largest spheres (i.e., maximal balls) one can insert into a configuration without contacting any particles.

We briefly describe the algorithm here as applied to a single configuration, and the reader is directed to Ref. 38 for further details as well as pictorial representations of the clustering algorithm.

The configuration is divided into a 3D grid and each point on the grid is tested for being filled or empty. A grid spacing of 0.2 was chosen to reduce the computational burden while still giving consistent results with finer spacing. If an *A* particle can be inserted at that point without experiencing a repulsive force from any other particle in the configuration, the point is empty. Otherwise, it is filled and cannot be the center of a maximal ball.

Let r_{AA}^0 be the separation of the pair potential minimum between two *A* particles and r_{AB}^0 be the corresponding separation for an *AB* pair. Also, let r_A be the distance of a grid point to the closest *A* particle and r_B be the distance to the closest *B* particle. If the grid point is empty, it is assigned a ball with radius r, where $r = \min\left\{r_A - \frac{r_{AA}^0}{2}, r_B - \frac{r_{AB}^0}{2}\right\}$. If for ball j there exists another ball i such that the distance between their centers $r_{ij} \leq r_i - r_j$, ball j is removed, as it is an inclusion of ball i. The remaining balls are the set of maximal balls for this configuration. Two balls i and j are defined as neighbors if they overlap, provided by the condition $r_{ij} < r_i + r_j$.

A distinct void is defined as a maximal ball where all of its neighboring maximal balls having smaller radii and the void radii we report below are the radii of these distinct voids. The connectivity of voids is determined through the following protocol. Starting from a distinct void, say void α, the first shell of neighboring maximal balls is identified, which are simply α's neighbors. The second shell of α identified as all neighbors of the first shell such that (a) it is not a member of the first shell and (b) a maximal ball in the second shell has a neighbor in the first shell with a larger radius. The third- and higher-order shells are identified in a similar manner until the search is exhausted, due to maximal balls in the final shell n having no new neighbors with smaller radii. All maximal balls in shells 1 to n are then labeled as the member of void α. This is done for each void. If there is a maximal ball that is a member of multiple voids, it is called a throat and marks the connection of at least two voids. The coordination number of a void is then defined as the number of unique voids with which it shares a common throat.

III. ATHERMAL FIRST-ORDER PHASE TRANSITIONS IN THE STRONG COHESION REGIME

In Fig. 2, we present the landscape equation of state $\langle P_{IS} \rangle$ and the corresponding average potential energy per particle $\langle e_{IS} \rangle$ for r_c values of 1.8 and 3.5, for system sizes $N = 500$; 1000; 2000; 8000; and 20 000. We have also performed the calculation for $N = 100\,000$ with $r_c = 1.8$. For the present discussion, this range of cutoffs (i.e., $r_c \geq 1.8$) constitutes what we will call the strong cohesion regime.

The behavior of this regime is consistent with our previous description of a cavitation transition in the energy landscape of simple cohesive liquids.[23] Our previous work[23] found that a Kob-Andersen 80:20 binary mixture[40] of both the (7, 6) and (12, 6) variants of Eq. (1) with $r_c = 3.5$ had landscape equations of state and $\langle e_{IS} \rangle$ with a similar response to system size as that
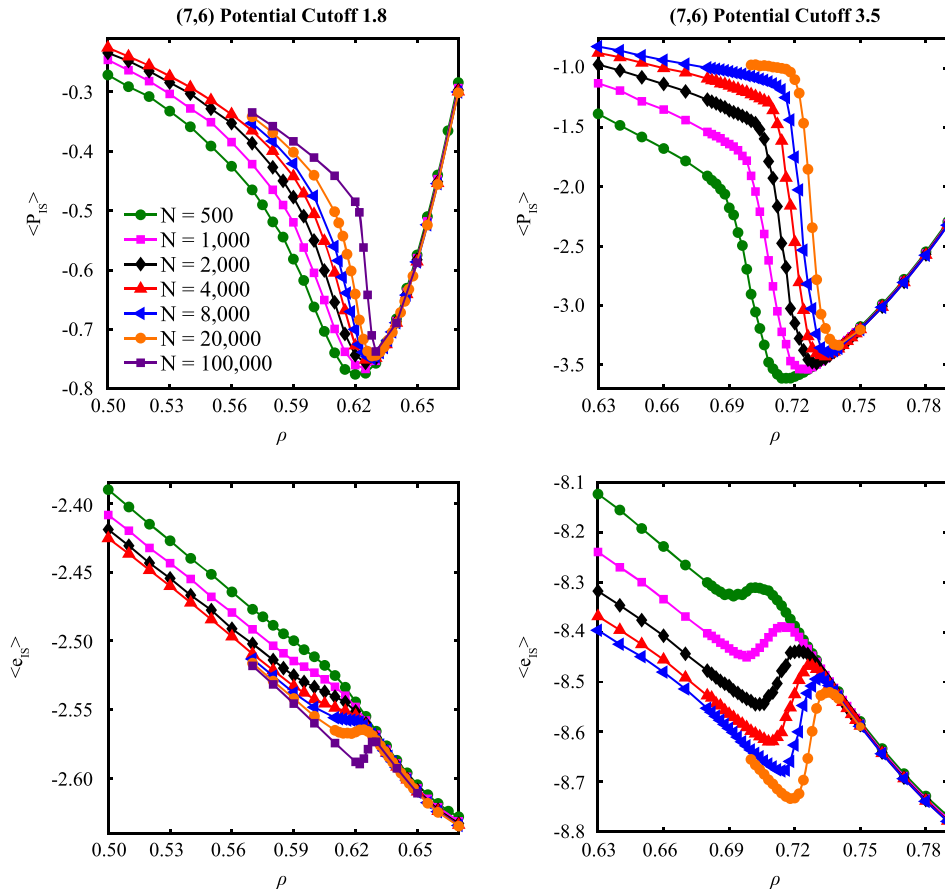
FIG. 2. Development of the landscape equation of state and the average potential energy per particle with system size for $r_c = 1.8$ and 3.5. This range of cohesive strengths ($r_c \geq 1.8$) exhibits strong finite-size affects, indicating the presence of a cavitation transition in the energy landscape.

of Fig. 2. While not shown, we observe a similar behavior for $r_c = 1.9$, 2.0, and 2.5.

A. Development of $\langle P_{IS} \rangle$ and $\langle e_{IS} \rangle$

This region of strong cohesion gives rise to landscape equations of state with a system-size response that suggests the existence of an athermal first-order phase transition. What appears to be a spinodal-like minimum at small system sizes develops toward becoming a discontinuous jump with increasing system size. Such a response is analogous to the finite-size rounding of first-order thermal phase transitions.[25–27] At small system size, the minimum at ρ_S represents the onset of cavitation. At ρ_S only a few liquid configurations cavitate upon energy minimization to produce inherent structures with significantly lower tension. The remainder are homogeneous and sustain high tension. As the density is reduced below ρ_S, the liquid progressively samples an increasing fraction of broken inherent structures, until all are fractured. This density range over which homogeneous and cavitated inherent structures are sampled is called the crossover region,[23] and its existence results in a smooth landscape equation of state for finite systems.

As the system size increases, the equation of state below the density of the minimum becomes steeper, while the width of the crossover region approaches zero. In the thermodynamic limit, ρ_S corresponds to a first-order phase transition in the energy landscape where the liquid transitions from sampling exclusively homogeneous to exclusively fractured inherent structures. The response in the equation of state is a

discontinuous jump from high to low tension. Evidently this range of cohesive strengths (i.e., $r_c \geq 1.8$) gives rise to the same transition in the energy landscape.

Like our previous characterization,[23] $\langle e_{IS} \rangle$ exhibits strong finite-size effects at densities below ρ_S. At large enough system sizes, both cohesive strengths contain a loop, as Fig. 2 clearly illustrates, with the two extrema delineating the range of the crossover region. In the thermodynamic limit, these curves are expected to likewise become discontinuous as the liquid transitions from exclusively sampling basins of attraction with minima that are homogeneous to ones that are fractured and at lower potential energy.

B. Development of the pressure distribution

In our previous work, we found that in a region below ρ_S the inherent structure pressure distribution was bimodal, indicating that the system was sampling a mixture of fractured (low-tension) and homogeneous (high-tension) inherent structures. As the liquid is decompressed below ρ_S, the low tension peak grows at the expense of the higher-tension one. Once all configurations cavitate upon minimization, the distribution is once again unimodal.

Figure 3 shows the development of the pressure distributions crossing the Sastry density ($\rho_S = 0.630$) for $r_c = 1.8$; $N = 100\,000$. This value of r_c marks the lower bound of cutoffs that still gives rise to the above-described phenomenology. Above ρ_S the distribution is narrow and unimodal. As the liquid is decompressed, the distribution develops a second, low-tension peak that grows upon further decompression. The
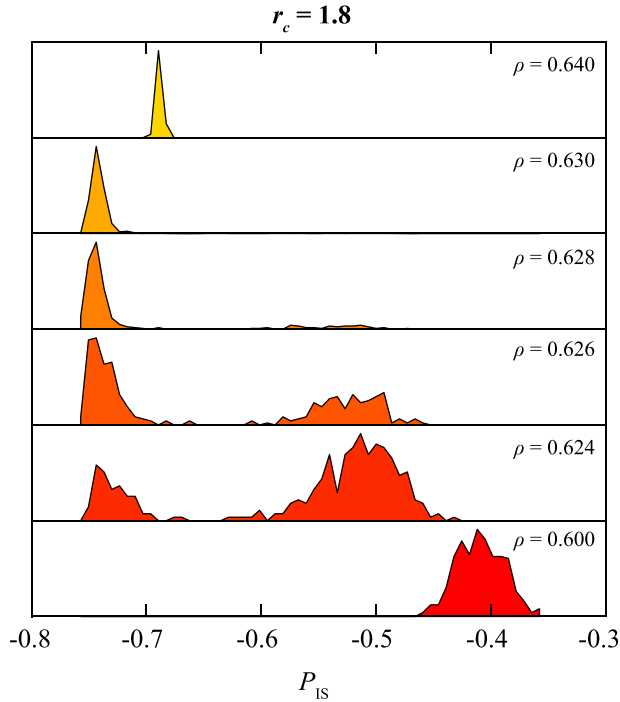
FIG. 3. Development of the inherent structure pressure distribution crossing the tensile instability at ρ_S for $r_c = 1.8$; $N = 100\,000$. Below ρ_S, the distribution becomes bimodal, as the liquid samples both homogeneous and fractured inherent structures. At low enough density, all the inherent structures are fractured, and the pressure distribution is unimodal.

distribution is again unimodal at low enough density. While we have only shown this development for $r_c = 1.8$, all of the more cohesive systems we have studied exhibit similar behavior at sufficiently large system size.

C. Finite-size scaling of the cavitation transition

The fact that for $r_c = 1.8$ the liquid samples two distinct inherent structure distributions in the crossover region allows us to perform a finite-size scaling analysis to estimate ρ_S in the thermodynamic limit. Like our previous study,[23] we detect the presence of voids by generating instantaneous interface representations[41] of the voids, which provides a set of points that defines the interface between the compact particle regions and the voids. Configurations are considered homogeneous if no interface is found, and fractured otherwise. The fraction of homogeneous inherent structures f_{homo} at a given ρ is fit to a sigmoidal curve, and this allows us to estimate $\rho_{1/2}$, the density where sampling homogeneous and fractured inherent structures is equally probable. For finite systems, $\rho_{1/2}$ is the nominal location of the phase transition and becomes equal to ρ_S in the thermodynamic limit.

Figure 4 suggests that the finite-system size deviation of $\rho_{1/2}$ from the $N \to \infty$ limit follows a $1/N^{1/3}$ scaling law for the cutoffs in this regime, in agreement with the scaling proposed in our earlier presentation of this transition.[23] We stress again here that this is an empirical result with no accompanying theory. Given the similarity in the behavior of the landscape equation of state and the same scaling relation, it appears that the same physics applies to this range of cohesive strengths, supporting the generality of the phenomenon we proposed
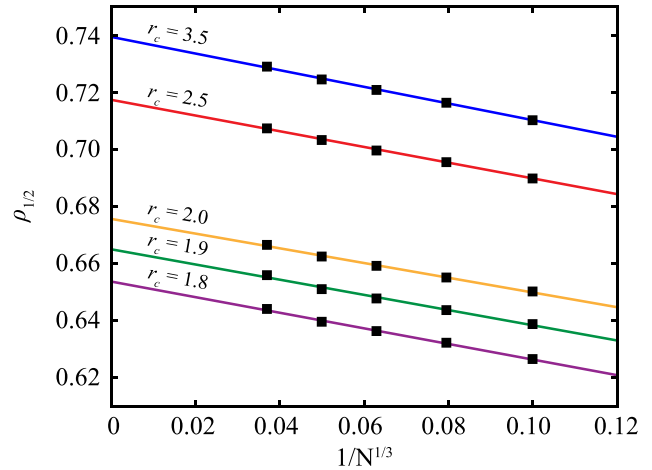
FIG. 4. Finite-size scaling of the cavitation transition for cutoffs within the strong cohesion regime.

earlier.[23] A cavitation transition in the energy landscape is found for $r_c \geq 1.8$.

D. Differences between cutoffs in the strong cohesion regime

With the above similarities noted, it is worth pointing out the differences among the varying cohesive strengths in this regime. As expected, the tensile strength of the liquid is reduced upon reducing the cutoff. For lower cutoffs in this regime, clear indications of a first-order phase transition are not apparent until appreciably larger system sizes than for higher cutoffs. For example, for $r_c = 3.5$ with $N = 500$, there is a "kink" in $\langle P_{IS} \rangle$ at a density below that of the minimum, which is where the crossover region ends, and the system exclusively samples the fractured branch. For $r_c = 1.8$, this signature is not observable until $N = 100\,000$. Thus, it may be that computational studies of the phase behavior and rheology of moderately attractive particles require substantially larger systems than required for simulations of more attractive liquids.

IV. WEAK COHESION REGIME

Figure 5 presents the landscape equations of state and $\langle e_{IS} \rangle$ for $r_c = 1.4$ and 1.7 for $N = 500$; 1000; 2000; 8000; $20\,000$, and $100\,000$. This range ($r_c = 1.4\text{-}1.7$) will be referred to as weak cohesion. As will now be shown, weaker cohesion displays qualitatively different behavior than the strong cohesion regime.

A. Behavior of averages

The landscape equations of state still exhibit minima, indicating the presence of a tensile instability. Though we will suggest that this tensile instability is different from that of the strong cohesion regime, we will continue to refer to its location as the Sastry point. Unlike the strong cohesion regime, $\langle e_{IS} \rangle$ does not develop extrema in the neighborhood of ρ_S. Rather, ρ_S appears to coincide with an inflection point in $\langle e_{IS} \rangle$.

The most notable difference from the strong cohesion regime is the minimal effect of finite-sizes, which are in fact
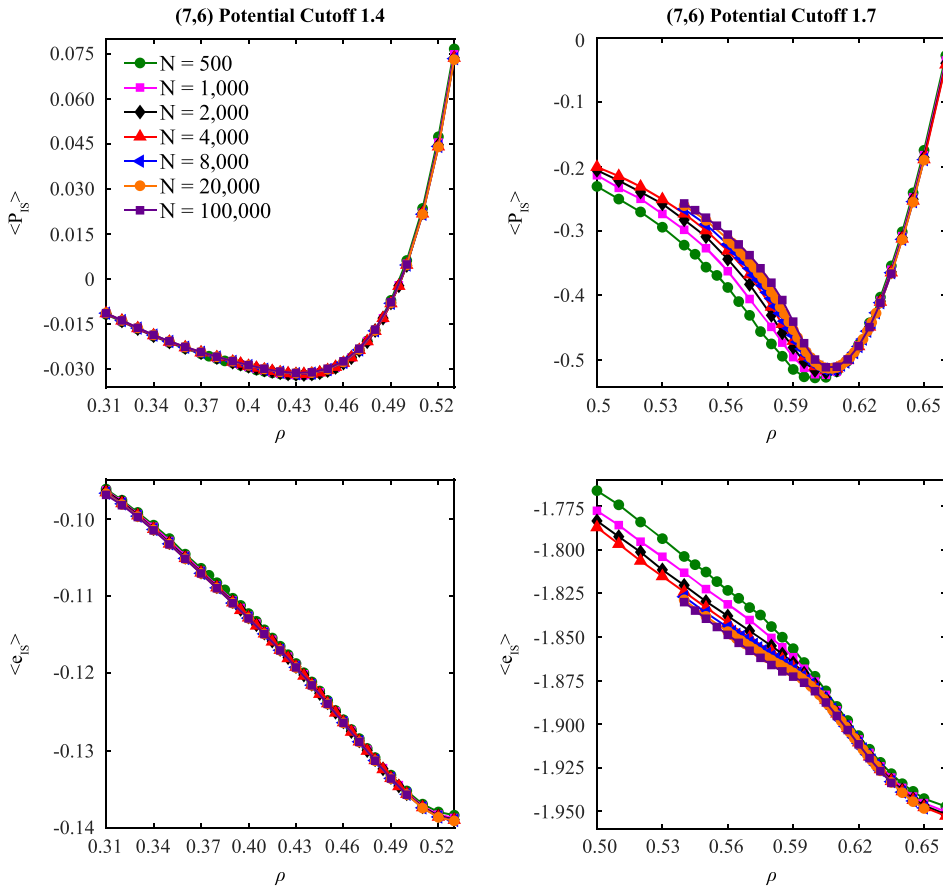
FIG. 5. Development of the landscape equation of state and the average potential energy per particle with system size for $r_c = 1.4$ and 1.7. This range of cohesive strengths ($1.4 \leq r_c \leq 1.7$) exhibits minimal finite-size effects yet still displays a tensile instability in the energy landscape.

entirely absent for $r_c = 1.4$. While $r_c = 1.7$ exhibits finite-size effects below ρ_S, the response is rather weak and appears to be converging with increasing N. In the thermodynamic limit, the shape of the landscape equation of state remains akin to a mean-field spinodal rather than a discontinuity. The tensile instability is not associated with an abrupt phase transition separating homogeneous and fractured inherent structures. Based on the landscape equation of state, it appears that the inherent structures start breaking at ρ_S and become progressively more broken as tension in the inherent structures is relieved upon decompression of the liquid. This is opposed to the mix of homogeneous and fractured inherent structures observed in the strong cohesion regime at finite sizes.

B. Pressure distributions

Such an interpretation is supported by considering the pressure distributions. Figure 6 presents the development of the pressure distributions for $r_c = 1.7$; $N = 100\,000$ as the system is decompressed below the tensile instability at ρ_S. This cutoff represents the most cohesive particles of the weak cohesion regime, and while not shown, the development of the pressure distributions for all cutoffs in this regime is akin to that in Fig. 6.

Unlike the strong cohesion regime, the pressure distribution remains unimodal as the entire peak moves to lower tensions below ρ_S. In this case, the peak develops a tail on the low tension side, and there is a range of densities where the distribution is much broader. However, at no point is there any

evidence that the liquid samples two distinct types of inherent structure, precluding any attempt to perform a finite-size scaling analysis. Rather than a discontinuous phase transition,
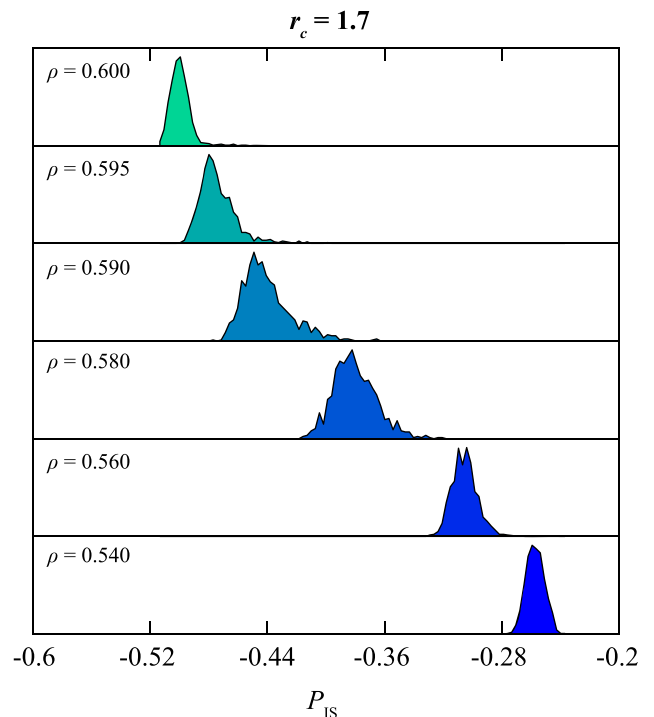
FIG. 6. Development of the inherent structure pressure distribution crossing the tensile instability at ρ_S for $r_c = 1.7$; $N = 100\,000$. Below ρ_S, the distribution remains unimodal, and the entire distribution shifts to lower tension.

the tensile instability for weak cohesion is more continuous in nature as the inherent structures gradually relieve tension.

V. VOID CHARACTERISTICS: DIFFERENCE BETWEEN STRONG AND WEAK COHESION

While both cohesive regimes contain tensile instabilities in the energy landscape, their response to system size is rather different. Specifically, the strong cohesion regime exhibits behavior akin to the athermal first-order phase transition we previously characterized,[23] while weak cohesion has a landscape equation of state that remains spinodal-like for all system sizes. To provide a structural basis for this difference, we have used Dong and Blunt's[38] modified maximal ball algorithm (described in Sec. II) to analyze how the void space in the inherent structures develops upon yielding.

A. Void size and multiplicity

Figure 7 shows the average void radius $\langle r \rangle$ and average number of voids per unit volume $\langle \bar{n}_{voids} \rangle$ for $r_c = 1.4$ and 3.5,

representing the extremes of cohesion we have considered in this work. For $r_c = 3.5$, the average pore radius departs from zero at ρ_S. Because there are only a few voids immediately below ρ_S, it would require many more configurations than we have produced to converge. Therefore, we only show the curves of $\langle r \rangle$ starting slightly below ρ_S. For strong cohesion, the typical radius increases with system size for each density. An interesting feature is that at large system sizes, $\langle r \rangle$ develops a maximum. Recall that the size shown represents the minor axis or narrowest dimension of a void. Upon inspection, we see that somewhat below ρ_S, larger system sizes exhibit voids that are more elongated and branched (Fig. 8 right). However, densities closer to ρ_S exhibit voids that are approximately spherical (Fig. 8 left). Such a development is reminiscent of the sphere to cylinder transition of bubbles seen in finite thermal systems.[24]

For $r_c = 1.4$, like the landscape equation of state, $\langle r \rangle$ contains no system size effects, and $\langle \bar{n}_{voids} \rangle$ is also system size independent. Evidently for weak cohesion, more voids of similar size are formed as a result of increasing system
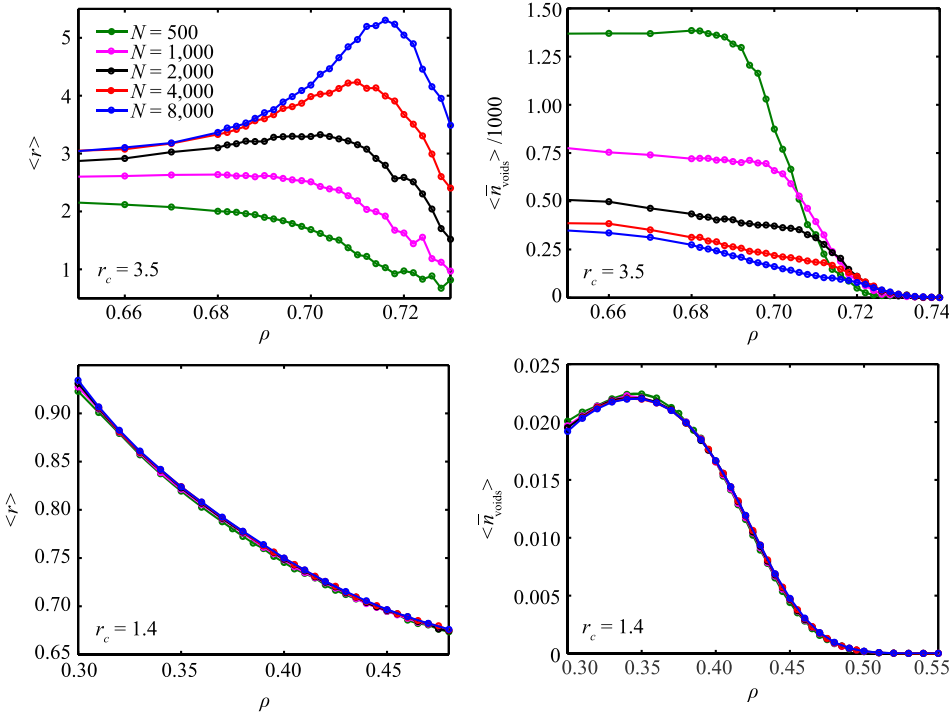
FIG. 7. Average void radius $\langle r \rangle$ and number of voids per unit volume $\langle \bar{n}_{voids} \rangle$ for $r_c = 1.4$ and 3.5.
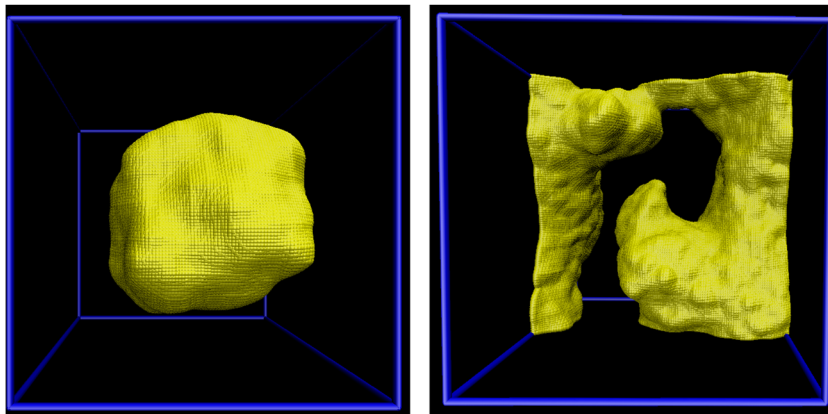
FIG. 8. Instantaneous interface representations of the void space that emerges upon energy minimization in strongly cohesive ($r_c = 3.5$) systems below ρ_S. The image on the left shows a typical void found just below ρ_S; it is a large, compact, and roughly spherical void. For larger system sizes, the average void size develops a maximum below ρ_S, which is due to the voids becoming elongated and branched. The image on the right shows an example of such a configuration for $N = 8000$ at $\rho = 0.62$.
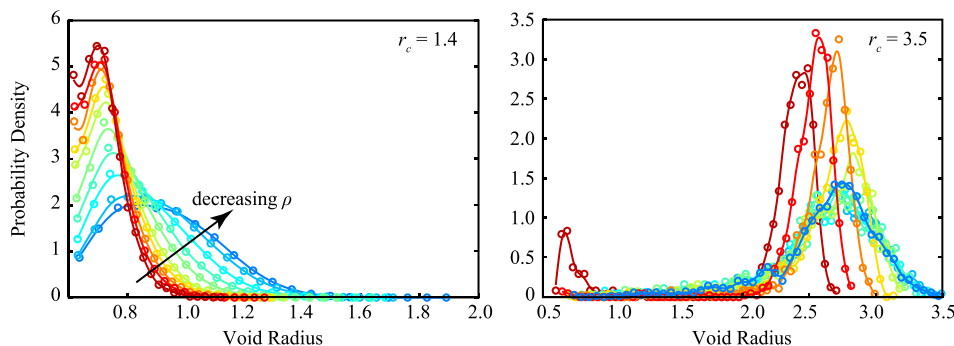
FIG. 9. Development of the void size distribution with density for $r_c = 1.4$ and 3.5 as the system is decompressed below ρ_S. The left panel displays densities between 0.30 and 0.43, specifically: 0.30, 0.31, 0.33, 0.35, 0.37, 0.39, 0.40, 0.41, 0.42, and 0.43. The right panel displays densities between 0.62 and 0.71, incremented by 0.01.

size, which in turn keeps the tension constant for a given density. On the other hand, $\langle \bar{n}_{voids} \rangle$ scaled by system volume for $r_c = 3.5$ decreases with system size, indicating that larger systems accommodate the additional volume by producing larger rather than more voids. This results in more tension being relieved as the system size increases at fixed density below ρ_S.

Figure 9 shows how the void size distribution develops below ρ_S for $r_c = 1.4$ and 3.5. Recall that the size shown represents the minor axis or narrowest dimension of a void. The more cohesive particles tend to have large voids narrowly distributed around the mean. The only exception is at the largest density shown, where there is also a second peak around 0.6 that disappears upon decompression. Such large voids are consistent with the phase transition in this regime being associated with catastrophic material failure.

Around the yielding point, the particles with weak cohesion ($r_c = 1.4$) contain small voids, ones that can accommodate the insertion of only a single particle. We have also performed the void analysis for the thermal liquid, and we observed voids with radii between 0.6 and 0.8. We stress that this is a result of density fluctuations in the liquid rather

than cavitation, as $\left(\frac{\partial P}{\partial \rho} \right)_T > 0$ over the entire density range considered, implying that some of these voids in the inherent structures are simply the result of density fluctuations in the liquid. As the density is reduced, this distribution develops a tail and broadens, as larger voids are produced through minimization. While this latter feature is not observed in the liquid, we do not observe separate distributions for voids already in the liquid and those created upon energy minimization. Thus, simply considering differences in void size is not sufficient to resolve how yielding occurs upon energy minimization.

B. Void connectivity associated with yielding for weakly cohesive particles

In contrast with the above-described behavior, we observe such resolution between features in the liquid and inherent structures by considering the connectivity of voids. In fact, as will be shown below, it appears that yielding in this regime of weak cohesion is the result of a highly connected network of small voids that emerges upon energy minimization.

Figure 10 shows the coordination number distribution for $r_c = 1.4$, $N = 1000$ at $\rho = 0.31$, a density well below ρ_S, for
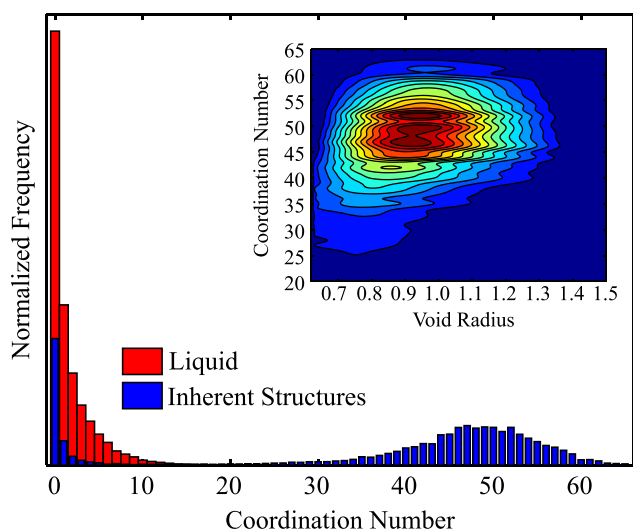
FIG. 10. Coordination number distribution of voids in the liquid and inherent structure for $r_c = 1.4$ at $\rho = 0.31$, a density well below ρ_S. Energy minimization results in the formation of a highly interconnected network of small voids. Plotting the joint probability distribution of void size and coordination number of the inherent structures (inset) results in an "island" at high coordination number and small radius that is absent in the liquid.
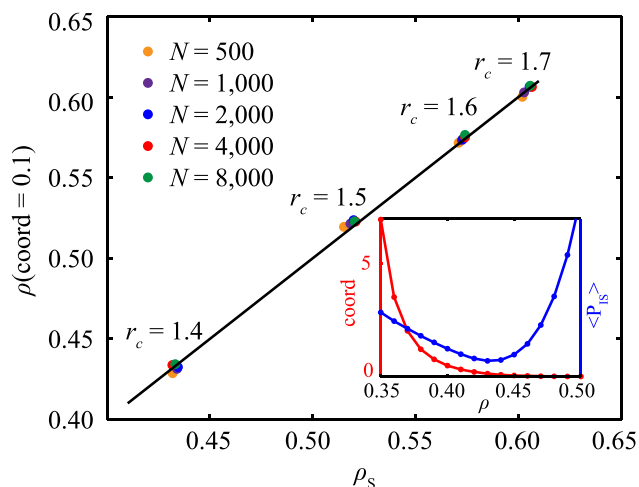
FIG. 11. The density where the average coordination number departs from zero (defined as 0.1) versus ρ_S, the density of tensile instability in the energy landscape, for cutoffs in the weakly cohesive regime. The coincidence of these two densities suggests that yielding in the energy landscape of weakly cohesive systems is due to the formation of a highly interconnected network of voids. The inset shows an example of the average coordination number plotted alongside the landscape equation of state for $r_c = 1.4$.
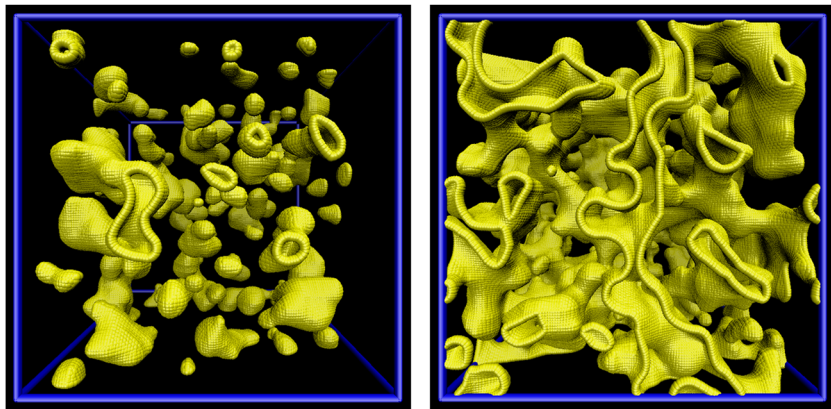
FIG. 12. Representations of the void space near and well below ρ_S for r_c = 1.4; N = 1000. The image on the left at ρ = 0.43 shows that there are many isolated voids. As the density is reduced to 0.31 (right image), the voids become highly interconnected.

both the thermal liquid and the underlying athermal inherent structures. While the method we have used recognizes voids in the liquid, they tend to be weakly if at all connected. Energy minimization results in a bimodal distribution, due to the emergence of a second peak at high coordination number. Producing the joint probability distribution of void size and coordination number results in an "island" (inset Fig. 10) at small pore size and large coordination number that does not exist in the liquid. Thus, energy minimization below ρ_S gives rise to a highly interconnected network of voids that is absent in the liquid, suggesting that either connectivity or the percolation of voids is responsible for the athermal tensile instability in weakly cohesive particles.

To further test this connection between yielding behavior and void connectivity, we have plotted ρ_S versus the density where the average coordination number departs from zero, defined as crossing 0.1, for all cutoffs and system sizes in the weak cohesion regime. Figure 11 displays these points along with the line y = x. All cutoffs in this regime display yielding precisely at the same density where this network begins to emerge. The inset shows the average coordination number and the landscape equation of state for r_c = 1.4; N = 8000 plotted simultaneously. While we do observe voids above ρ_S, their average coordination number departs from zero at the tensile instability. We stress that the development of this network is gradual for all system sizes. Thus, yielding for weakly cohesive particles does not behave like a first-order phase transition with coordination number as the order parameter. Rather, ρ_S is associated with the onset of formation of a highly connected network of voids, regardless of system size.

Figure 12 shows an image of the void space at ρ = 0.43, approximately ρ_S, and at lower density ρ = 0.31 for r_c = 1.4, N = 1000. Note that the images produced are sensitive to the parameters used in the instantaneous interface protocol[41] (e.g., coarse-graining length). While this qualitative description of transitioning from an isolated to highly connected void network remains intact, the size, multiplicity, and connectivity of voids will change depending on one's choice of parameters. As suggested by the void analysis above, around the tensile instability, voids exist in the inherent structures, yet they are largely isolated. At reduced density, the network becomes highly interconnected, a feature seen only in the inherent structures.

VI. CONCLUDING REMARKS

Here, we have shown that cohesion among particles results in a tensile instability in the energy landscape. However, this tensile instability behaves qualitatively differently depending on the strength of cohesion. We have identified two cohesive regimes: a strongly cohesive and a weakly cohesive regime. The former exhibits an athermal first-order phase transition,[23] where in the thermodynamic limit, the system transitions abruptly at ρ_S from exclusively homogeneous inherent structures under large isotropic tension to fractured inherent structures with large voids at significantly reduced tension. While the landscape equation of state appears to be passing through a spinodal at small system sizes, it becomes discontinuous in the thermodynamic limit.

Weakly cohesive particles also contain a tensile instability in the energy landscape. However, its response to system size is minimal or absent. The tensile instability in this case is associated with the emergence of a highly interconnected network of small voids. Rather than an abrupt phase transition, this transition is continuous and remains so in the thermodynamic limit. Such a response leaves open the possibility that the precise descriptions of yielding in systems of weakly cohesive particles should be that of a higher-order phase transition. Given that this behavior applies to particles with rather weak interactions, there may be limited applicability of the jamming picture[6,8] to particles with cohesion, contrary to suggestions that attractions can be treated as a perturbation of the jamming of granular materials.[42,43]

The picture we have developed here enriches our understanding of yielding in systems of cohesive particles as viewed through the perspective of the energy landscape. While we have sampled the energy landscape along a high temperature isotherm, performing athermal expansions (as in Ref. 23) within the weakly cohesive regime would serve as a useful complement. It is expected that the weakly attractive regime will be important for interpreting the tensile behavior of colloids and perhaps amorphous protein aggregates. The principles outlined here may also apply to the study of brittle failure, which is often associated with the nucleation of small cavities. While some have considered the role of disorder[44] and rigidity,[45] there appears to have been less consideration of cohesive strength. As suggested by the present work, there is distinct yielding behavior depending on the cohesive strength,

suggesting it may be an important variable in the study of brittle failure.

ACKNOWLEDGMENTS

[1] J. D. Weeks, D. Chandler, and H. C. Andersen, J. Chem. Phys. **54**, 5237 (1971).

[2] H. C. Andersen, D. Chandler, and J. D. Weeks, Adv. Chem. Phys. **34**, 105 (1976).

[3] F. H. Stillinger and T. A. Weber, Phys. Rev. A **25**, 978 (1982).

[4] F. H. Stillinger and T. A. Weber, Science **225**, 983 (1984).

[5] F. H. Stillinger, *Energy Landscapes, Inherent Structures, and Condensed-Matter Phenomena* (Princeton University Press, Princeton, 2016).

[6] A. J. Liu and S. R. Nagel, Nature **396**, 21 (1998).

[7] C. S. O'Hern *et al.*, Phys. Rev. Lett. **88**, 075507 (2002).

[8] C. S. O'Hern *et al.*, Phys. Rev. E **68**, 011306 (2003).

[9] A. J. Liu and S. R. Nagel, Annu. Rev. Condens. Matter Phys. **1**, 347 (2010).

[10] C. P. Goodrich, A. J. Liu, and S. R. Nagel, Phys. Rev. Lett. **109**, 095704 (2012).

[11] P. G. Debenedetti *et al.*, J. Phys. Chem. B **103**, 7390 (1999).

[12] D. S. Corti *et al.*, Phys. Rev. E **55**, 5522 (1997).

[13] S. Sastry *et al.*, Phys. Rev. E **56**, 5524 (1997).

[14] S. Sastry, Phys. Rev. Lett. **85**, 590 (2000).

[15] E. La Nave *et al.*, J. Chem. Phys. **120**, 6128 (2004).

[16] J. Hernandez-Rojas and D. J. Wales, Phys. Rev. B **68**, 144202 (2003).

[17] R. A. Laviolette, Phys. Rev. B **40**, 9952 (1989).

[18] M. Utz, P. G. Debenedetti, and F. H. Stillinger, J. Chem. Phys. **114**, 10049 (2001).

[19] V. K. Shen, P. G. Debenedetti, and F. H. Stillinger, J. Phys. Chem. B **106**, 10447 (2002).

[20] R. A. La Violette, J. L. Budzien, and F. H. Stillinger, J. Chem. Phys. **112**, 8072 (2000).

[21] C. J. Roberts, P. G. Debenedetti, and F. H. Stillinger, J. Phys. Chem. B **103**, 10258 (1999).

[22] F. H. Stillinger, P. G. Debenedetti, and T. M. Truskett, J. Phys. Chem. B **105**, 11809 (2001).

[23] Y. E. Altabet, F. H. Stillinger, and P. G. Debenedetti, J. Chem. Phys. **145**, 211905 (2016).

[24] L. G. MacDowell, V. K. Shen, and J. R. Errington, J. Chem. Phys. **125**, 034705 (2006).

[25] L. G. MacDowell *et al.*, J. Chem. Phys. **120**, 5293 (2004).

[26] M. Schrader, P. Virnau, and K. Binder, Phys. Rev. E **79**, 061104 (2009).

[27] K. Binder *et al.*, Am. J. Phys. **80**, 1099 (2012).

[28] M. H. J. Hagen *et al.*, Nature **365**, 425 (1993).

[29] M. H. J. Hagen and D. Frenkel, J. Chem. Phys. **101**, 4093 (1994).

[30] Z. Shi *et al.*, J. Chem. Phys. **135**, 084513 (2011).

[31] G. Wahnström, Phys. Rev. A **44**, 3752 (1991).

[32] S. Plimpton, J. Comput. Phys. **117**, 1 (1995).

[33] S. Nose, J. Chem. Phys. **81**, 511 (1984).

[34] W. G. Hoover, Phys. Rev. A **31**, 1695 (1985).

[35] E. Polak and G. Ribiere, Rev. Fr. Inf. Rech. Opérationnelle **3**, 35 (1969).

[36] W. Humphrey, A. Dalke, and K. Schulten, J. Mol. Graphics **14**, 33 (1996).

[37] F. H. Stillinger, Phys. Rev. E **59**, 48 (1999).

[38] H. Dong and M. J. Blunt, Phys. Rev. E **80**, 036307 (2009).

[39] D. Silin and T. Patzek, Phys. A **371**, 336 (2006).

[40] W. Kob and H. C. Andersen, Phys. Rev. E **51**, 4626 (1995).

[41] A. P. Willard and D. Chandler, J. Phys. Chem. B **114**, 1954 (2010).

[42] N. Xu *et al.*, Phys. Rev. Lett. **98**, 175502 (2007).

[43] C. P. Goodrich, A. J. Liu, and S. R. Nagel, Nat. Phys. **10**, 578 (2014).

[44] A. Shekhawat, S. Zapperi, and J. P. Sethna, Phys. Rev. Lett. **110**, 185505 (2013).

[45] M. M. Driscoll *et al.*, Proc. Natl. Acad. Sci. U. S. A. **113**, 10813 (2016).